NON-THERMAL PROCESSES IN LARGE SOLAR FLARES

R. P. LIN

Space Sciences Laboratory, University of California, Berkeley, California 94720

and

H. S. HUDSON

Physics Department, University of California, La Jolla, California 92037

(Received 2 February; in revised form 11 May, 1976)

Abstract. We analyze particle acceleration processes in large solar flares, using observations of the August, 1972, series of large events. The energetic particle populations are estimated from the hard X-ray and γ-ray emission, and from direct interplanetary particle observations. The collisional energy losses of these particles are computed as a function of height, assuming that the particles are accelerated high in the solar atmosphere and then precipitate down into denser layers. We compare the computed energy input with the flare energy output in radiation, heating, and mass ejection, and find for large proton event flares that:

(1) The ~ 10-10^2 keV electrons accelerated during the flash phase constitute the bulk of the total flare energy.

(2) The flare can be divided into two regions depending on whether the electron energy input goes into radiation or explosive heating. The computed energy input to the radiative quasi-equilibrium region agrees with the observed flare energy output in optical, UV, and EUV radiation.

(3) The electron energy input to the explosive heating region can produce evaporation of the upper chromosphere needed to form the soft X-ray flare plasma.

(4) Very intense energetic electron fluxes can provide the energy and mass for interplanetary shock wave by heating the atmospheric gas to energies sufficient to escape the solar gravitational and magnetic fields. The threshold for shock formation appears to be $\sim 10^{31}$ ergs total energy in >20 keV electrons, and all of the shock energy can be supplied by electrons if their spectrum extends down to 5–10 keV.

(5) High energy protons are accelerated later than the 10–10^2 keV electrons and most of them escape to the interplanetary medium. The energetic protons are not a significant contributor to the energization of flare phenomena. The observations are consistent with shock-wave acceleration of the protons and other nuclei, and also of electrons to relativistic energies.

(6) The flare white-light continuum emission is consistent with a model of free-bound transitions in a plasma with strong non-thermal ionization produced in the lower solar chromosphere by energetic electrons. The white-light continuum is inconsistent with models of photospheric heating by the energetic particles. A threshold energy of $\sim 5 \times 10^{30}$ ergs in >20 keV electrons is required for detectable white-light emission.

The highly efficient electron energization required in these flares suggests that the flare mechanism consists of rapid dissipation of chromospheric and coronal field-aligned or sheet currents, due to the onset of current-driven Buneman anomalous resistivity. Large proton flares then result when the energy input from accelerated electrons is sufficient to form a shock wave.

1. Introduction

Large solar flares may release as much as 10^{32} to 10^{33} ergs in a time scale of order 10^3 seconds. This energy appears in the form of electromagnetic radiation over the entire spectrum from γ-rays to radio burst, in fast electrons and nuclei up to relativistic energies, in the creation of a hot coronal cloud, and in large-scale mass

Solar Physics **50** (1976) 153–178.

motions including the ejection of material from the Sun. Although each of these phenomena has been studied in some detail, the primary energy release mechanism for solar flares is not well understood.

Non-thermal processes provide an important clue to the nature of the flare energy-release mechanism. In many small solar flares non-relativistic electrons accelerated during the initial phase constitute the bulk of the total flare energy output (Lin and Hudson, 1971). Thus the basic energy release mechanism of these flares essentially converts the available flare energy into fast electrons. These electrons may produce much of the observed flare emission in the X-ray, EUV, optical and radio regions through their various interactions with the solar atmosphere (e.g., Kane, 1974). This paper examines the significance of particle acceleration processes in large solar flares, and the importance of the accelerated particles in the generation of other phenomena in such flares. The analysis is oriented towards showing the energetic feasibility of the processes we describe rather than proving their necessity.

We use the comprehensive observations of the August 1972 series of large flares to obtain quantitative estimates of the energetic particle populations, the electromagnetic emissions and the mass ejections. The fluxes of energetic electrons and protons are derived from the observed X-ray and γ-ray emissions, respectively. Then the energy input into the solar atmosphere from the collisional losses of these energetic particles is computed as a function of overlying column density, under the assumption that particles are accelerated at a point high in the solar atmosphere and then precipitate into the corona and chromosphere (Hudson, 1972, 1973; Brown, 1973b). We then compare this energy input with the various observed flare energy outputs: radiation, mass ejection and shock wave formation, and energetic particles emitted into the interplanetary medium.

We find that these comparisons yield results similar to those obtained in our earlier paper (Lin and Hudson, 1971) and show the energetic dominance of non-relativistic electrons in large proton flares. We find that the flash phase radiation, the soft X-ray flare plasma, and the interplanetary shock wave can be consistently and quantitatively explained as the result of the interaction of these electrons with the solar atmosphere. On the other hand the energetic protons and other nuclei appear not to contribute significantly to the energization of flare phenomena, and the bulk of these particles appear to have been accelerated by the shock wave.

Finally we discuss the implication of these comparisons on theories of flares and particle acceleration, and on energy release mechanisms in solar flares.

2. Observations

The large flare events of August, 1972, including the largest energetic proton event of the past solar cycle, originated in McMath plage region No. 11976. Solar and interplanetary observations for the period 31 July to 11 August appear in the

TABLE I
Major non-thermal flare events McMath plage 11976 August 2–7, 1972

1. Hα flare						
date	2 Aug	2 Aug	2 Aug	4 Aug	7 Aug	7 Aug
start (UT)	0316	1839	1958	0617	0252	1449
max	(0327–0515)	1844	2058	0640	0255	1534
end	0800	1857	2336	0855	0320	1721
location	N14 E34	N14 E26	N14 E28	N14 E08	N15 W30	N14 W37
2. >20 keV X-ray bursts						
max U.T.	0330	1840	2046 and 2142	0625	0252	1521
>20 keV flux $(cm^2\ sec)^{-1}$	2×10^2	9×10^2	— and 3×10^2	4×10^3	3.5×10^2	7×10^3
3. Gamma ray emission						
observed lines (MeV)	—	—	(0.51)	0.51, 2.24, 4.4, 6.1		0.51, 2.24
4. Radio bursts						
μ-wave (10 cm) max UT	0405	1810	2148	0636	0253	1527
max flux $(10^{-22}$ W $m^{-2}\ Hz^{-1})$	2200	600	9300	7500	40	3900
metric, specral type	III, IV	IV	II[a], III, IV	II[a], III, IV	—	II, III, IV
5. Energetic particle						
max flux $(cm^2\ sr\ sec)^{-1}$						
>10 MeV protons	$\gtrsim5\times10^{2}$[b]	—	3×10^{3}[b]	2.5×10^4	—	10^3
>20 keV electrons	$\gtrsim6\times10^2$	—	$\gtrsim3.5\times10^3$	3×10^5		-1.5×10^4
6. Interplanetary shock wave, arrival UT						
at Earth	0119 (8/4)		0220 (8/4)	2354 (8/4)		0037 8/9)
at 0.78 AU (Pioneer 9)	0440 (8/3)		1117 (8/4)	2323 (8/4)		0707 (8/9)

[a] Possible type II's on August 2 and 4, reported in World Data Center "A", UAG-28 by Maxwell and Böhm and Krüger.
[b] At Pioneer 9, 0.78 AU and 40° east of Sun–Earth line.

comprehensive World Data Center "A" report UAG-28, "Collected data reports on August 1972 solar terrestrial events," and in the Solar Geophysical Data monthly reports. Table I and Figure 1 summarize these data, emphasizing the non-thermal observations. The energetic particle observations show that there were four major injections of particles into the interplanetary medium. The first two injections (2 Aug. ~0330 and ~2100 UT) were difficult to resolve from near-Earth observations because of the slow rise in the fluxes typical of events from eastern hemisphere flares. However, observations from the Pioneer 9 spacecraft, located at 0.78 AU radial distance and about 47° east of the Sun–Earth line, showed impulsive injection profiles for those two events (Roelof *et al.*, 1974). Each of these four injections of energetic particles was associated with a large bright flare and was accompanied by an intense hard (>20 keV) X-ray burst. In addition for the largest two flare events, those of 4 and 7 August, γ-ray line emissions from the Sun were detected for the first time (Chupp *et al.*, 1973).

These same four flare events apparently gave rise to the four interplanetary shock waves observed by Pioneer 9 and 0.78 AU and by other spacecraft near the Earth. Type II bursts accompanied three of the four events.

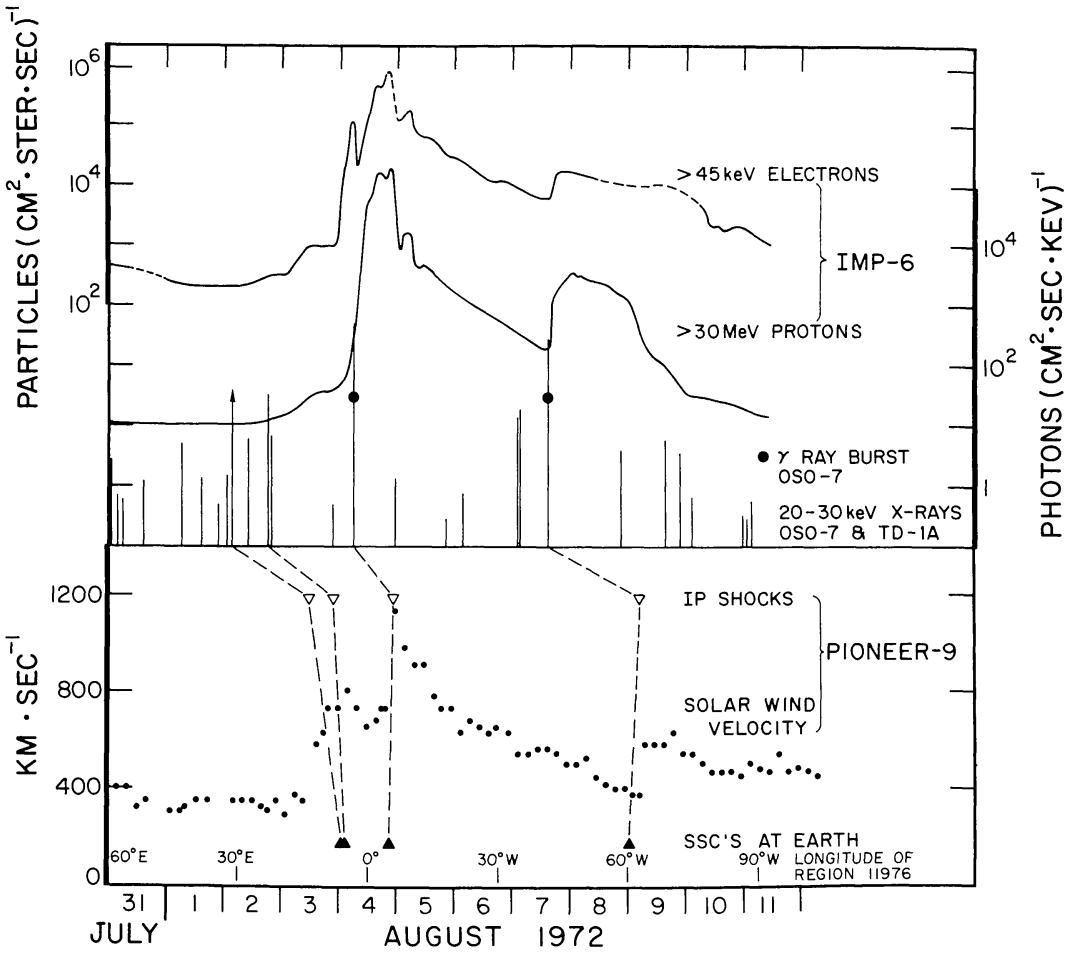

Fig. 1. A summary of solar non-thermal phenomena for the 31 July–11August 1972 period, taken from the World Data Center "A" report UAG-28 and *Solar Geophysical Data* monthly reports. Except for the Pioneer 9 plasma observations at 0.78 AU all the data are from Earth-orbiting spacecraft. Note the correspondence between energetic particle injections, shock waves, γ-ray bursts, and intense hard X-ray bursts.

3. The Energetic Particle Populations

The number and energy spectrum of the energetic particles at the Sun can be estimated, under certain assumptions, from the X-ray and γ-ray observations. In particular since these emissions arise from collisional processes – bremsstrahlung and nuclear collisions, respectively – the Coulomb collisional energy loss of these particles in the solar atmosphere can be derived. We will assume that all the X-ray and γ-ray emissions are produced by particles which stop in the solar atomosphere, i.e., thick target emission, and none by particles escaping to the interplanetary medium. This assumption clearly maximizes the depth of the collisional energy input in the solar atmosphere. Later we obtain a check on the validity of our assumptions by comparing the escaping particle population, as determined by direct interplanetary observations, with the particle population at the Sun, as deduced from our calculations.

Suppose the energetic particle source spectrum is given by dN/dE; then the

resulting total thick-target photon spectrum will be

$$\frac{dQ}{d(h\nu)} = \int_0^\infty dE \frac{d\sigma}{d(h\nu)}(E, h\nu)\left(\frac{dE}{d\xi}\right)^{-1} f\eta \int_E^\infty \frac{dN}{dE'} dE', \tag{1}$$

where $dQ/d(h\nu)$ = photon production rate per unit energy, $h\nu$ = photon energy, f = fractional abundance of the relevant ion, $d\sigma/d(h\nu)$ = differential cross section, $dE/d\xi$ = energy loss per g/cm^2 of material, η = Avogadro's number.

For bremsstrahlung from non-relativistic electrons in hydrogen ($f = 1$), the Bethe–Heitler approximation to the cross-section is satisfactory (Jackson, 1962):

$$\frac{d\sigma}{d(h\nu)}(E, h\nu) = 1.58 \times 10^{-24} \frac{1}{Eh\nu} \times$$

$$\times \ln\left[\left(\frac{E}{h\nu}\right)^{1/2} + \left(\frac{E}{h\nu} - 1\right)^{1/2}\right] \quad \text{cm}^2\,\text{ion}^{-1}\,\text{keV}^{-1} \quad \text{for } h\nu \leq E \tag{2}$$

$$= 0 \qquad \text{for } h\nu > E,$$

where E and $h\nu$ are in keV.

The energy loss rate is given by Trubnikov (1965):

$$\frac{dE}{d\xi} = 1.55 \times 10^5\, E^{-1} (\text{keV g}^{-1}\,\text{cm}^2), \tag{3}$$

Following the procedure of Brown (1971) we invert Equation (1) for a power-law energy spectrum to obtain

$$\frac{dN}{dE} = 5.9 \times 10^{33}\, b(\gamma) A \Delta t E^{-\gamma-1} \quad \text{electrons/keV}, \tag{4}$$

where $b(\gamma) = \gamma^2(\gamma-1)^2 B(\gamma - \frac{1}{2}, \frac{3}{2})$, and where $(dJ/d(h\nu))\,\Delta t = (1/4\pi R^2)(dQ/d(h\nu)) = A\Delta t E^{-\gamma}$, is the time-integrated X-ray spectrum observed at the orbit of the Earth, $R = 1$ AU, and $B(x,y)$ is the Beta function. The function $b(\gamma)$ is plotted in Figure 2. This expression differs from that of Brown (1971) because of the omission of a factor of π in his derivation (Hoyng and Brown, private communication) and the use of a different energy-loss rate. Table II gives the total number of electrons above 20 keV (the electron spectral exponent is $-\gamma - 1$) for the six largest hard X-ray bursts, including all the proton flares except the 2046 UT, 2 August event for which quantitative X-ray information is not available.

For γ-ray line emission from collisions with nuclei whose abundance fraction is f,

$$\frac{d\sigma}{d(h\nu)}(E, h\nu) = \sigma(E)\delta(h\nu - E_0)$$

and

$$N_\gamma = E_0 = f\eta \int_0^\infty dE \left(\frac{dE}{d\xi}\right)^{-1} \sigma(E) \int_E^\infty \frac{dN}{dE'} dE'. \tag{5}$$

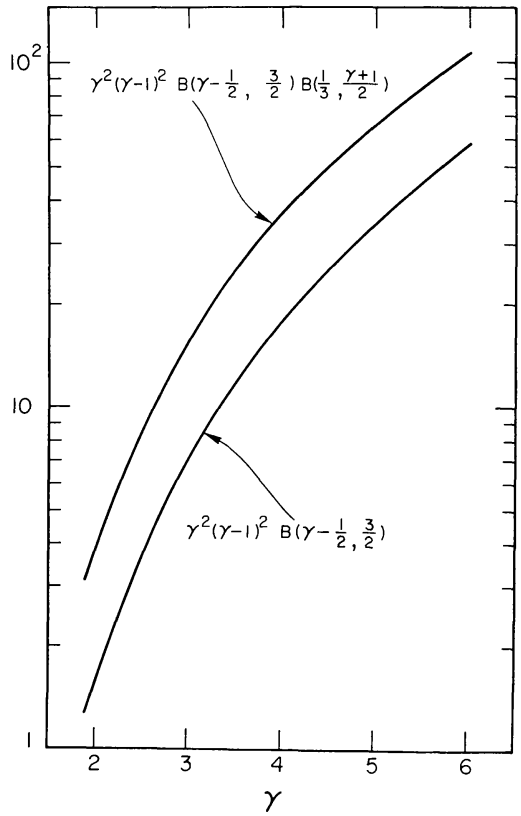

Fig. 2. The lower curve is a plot of $b(\gamma)$ for equation (4) of the text and the upper curve is a plot of $C(\gamma)$ for Equation (8) in the text.

TABLE II

Energetic particle populations August 2–7, 1972, non-thermal flare events

Event date	UT	Hard X-rays: burst parameters[a] A_m $(cm^2\ s\ keV)^{-1}$	γ_m	Δt	Energetic electrons: number >10 MeV at the flare[b]	escaping to the IP medium[c]	Total energy >20 keV (ergs)	Energetic electrons: number >20 keV at the flare[d]	escaping to the IP medium[c]	Total energy >10 MeV (ergs)
2 August	0330	7×10^6	4.1	≥260	2.5×10^{38}	$>5\times10^{33}$	1×10^{31}	NA	1×10^{34}	2×10^{29}
	1840	3.5×10^5	2.8	32	3×10^{37}	—	1.5×10^{30}	NA	—	
	2142	4.5×10^4	2.5	~600	1.5×10^{38}	$>3\times10^{34}$	8×10^{30}	NA	5×10^{34}	10^{30}
4 August	0625	1.2×10^6	2.7	500	2×10^{39}	2.5×10^{36}	1.1×10^{32}	6×10^{33}	5×10^{35}	8×10^{30}
7 August	0252	2×10^5	2.9	43	2×10^{37}	—	9×10^{29}	NA	—	
	1521	4.5×10^5	2.3	≥310	1×10^{39}	1×10^{35}	6×10^{31}	$>8\times10^{32}$	2×10^{34}	3×10^{29}

[a] The X-ray spectrum at burst maximum is $dJ/d(h\nu) = A_m(h\nu)^{-\gamma_m}$, and Δt is the effective duration at maximum flux. Except for OSO-7 observations of 2142 UT 2 August all X-ray observations are from ESRO TD-1.

[b] The electron spectrum can be obtained from the X-ray parameters with Equation (4).

[c] Because the 2 August flares are from E30 longitude, the electron estimates given here from near-Earth observations are low. The protons are estimated from Pioneer 9, at ~45° east of the Sun – Earth line.

[d] For the 1521 UT 7 August event only the end of the γ-ray event was observed by OSO-7.

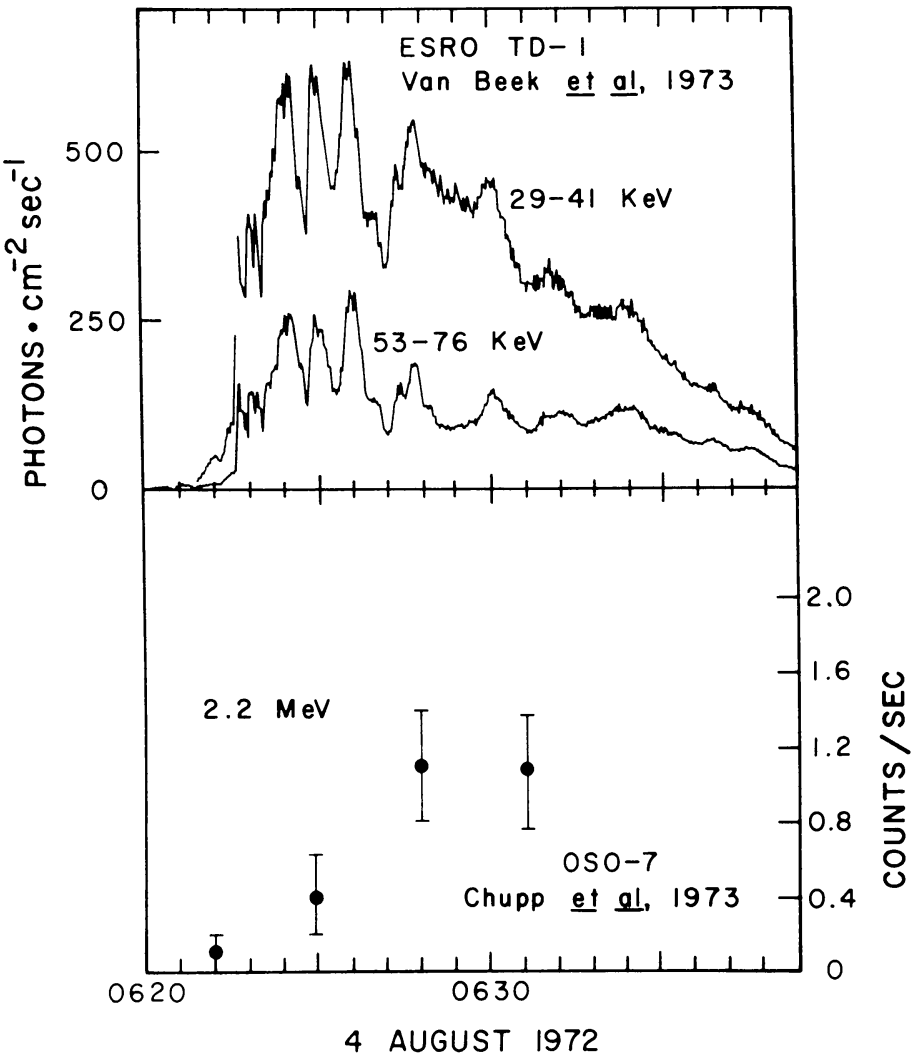

Fig. 3. The temporal evolution of the hard X-ray and 2.2 MeV γ-ray bursts for the 4 August 1972 flare is shown here. Note that the maximum of the γ-ray emission lags the X-ray maximum by several minutes.

Relatively complete γ-ray observations were available only for the 4 August flare. Figure 3 shows the X-ray and γ-ray time histories from the ESRO TD-1 (Hoyng, 1975) and OSO-7 (Chupp *et al.*, 1973) spacecraft respectively. The energetic proton spectrum can be obtained by comparing the γ-ray line emissions at 2.23 and 4.43 MeV (Ramaty and Lingenfelter, 1974). The 4.43 MeV line results from the prompt de-excitation of an excited level of C^{12}. The 2.23 MeV line results from neutron capture by hydrogen and subsequent de-excitation of deuterium. The neutrons are produced by the energetic protons interacting with a number of different nuclei. Detailed calculations of neutron propagation, taking into account both escape and non-radiative capture by He^3, have been performed to obtain the 2.23 MeV photon yield (Wang and Ramaty, 1974).

For 4 August the average 2.23 MeV γ-ray intensity was 0.3 photons $cm^{-2}\,sec^{-1}$ over the observation interval 0623–0633 UT and the ratio $N_\gamma(4.43)/N_\gamma(2.23) = 0.11 \pm 0.04$. Under the assumptions of a power law proton

spectrum and a thick target, Ramaty and Lingenfelter (1975) found a proton spectrum

$$\frac{dN}{dE} = 1.3 \times 10^{36} E^{-2.7 \pm 0.2} \text{ protons/MeV}.$$

For a thin target the spectral exponent would be -1.8 ± 0.2. Except for very steep proton spectra (power law index $\gtrsim 5$) the strongest γ-ray lines are produced primarily by protons above ~ 7 MeV. In the following discussion we will assume that the derived proton spectrum extends to energies below 7 MeV, following the power law determined by the γ-ray line ratio.

The total collisional energy losses of the energetic protons and electrons for the thick target case are then computed simply by

$$\varepsilon_{\text{coll}}(>E_0) = \int_{E_0}^{\infty} \frac{dN}{dE} E \, dE. \tag{6}$$

3.1. Particles escaping to the interplanetary medium

The numbers of protons and electrons escaping from the Sun can be derived from direct spacecraft observations. The angular and radial extent of the cone of field lines in the interplanetary medium filled with particles was estimated from observations on the Pioneer 9 and 10 plus near-Earth observations from IMP-6 (Roelof *et al.*, 1974) to be about 10^2 degrees and about 1.5 AU, respectively, giving a total volume of $V \approx 10^{40}$ cm^3. Then the total energy is just

$$\varepsilon_{\text{escape}}(>E_0) = V \int_{E_0}^{\infty} \frac{dJ}{dE} \frac{4\pi E}{v} dE. \tag{7}$$

These numbers are given in Table II.

Note that for the protons $\varepsilon_{\text{escape}} \approx 10^2 \varepsilon_{\text{coll}}$, i.e., most of the energetic protons either escaped to the interplanetary medium or were accelerated there. The spectrum of the energetic protons at 1 AU was approximately $\sim E^{-2}$ in the energy range $\sim 10 - 10^2$ MeV, closer to the thin-target interpretation of the 4.43/2.23 MeV γ-ray line ratio than the thick target. The observations therefore indicate that the γ-rays originated in thin-target emission as the energetic protons escaped from the Sun.

In addition, the 2.23 MeV γ-ray line emission peaks substantially later than the X-ray emission (Figure 3). Using a Monte Carlo calculation which takes into account the neutron capture time, Ramaty and Wang (1975) found the time profile of 2.2 MeV γ-ray emission is best fit under the assumption that the bulk of the protons is accelerated several minutes *after* the hard X-ray flash phase, and at the same time as the relativistic electrons. A second acceleration phase where relativistic electrons are accelerated has been observed for other large protons flares (Frost and Dennis, 1973; Frost, 1974).

The interplanetary electron observations show that $\leqslant 0.1\%$ of the electrons escape, consistent with the thick-target hypothesis. However, we cannot rule out the possibility that a large fraction of the electrons escape into the upper corona, where they become trapped in a region of low enough density to produce little bremsstrahlung. Some evidence for coronal trapping has been presented by Brown and Hoyng (1975) for the 4 August 1972 event.

We note that the total energy in >20 keV electrons is about 10^{32} ergs for the 4 and 7 August large flares. Since the electron spectrum may extend to well below 20 keV the total energy in fast electrons may substantially exceed 10^{32} ergs for these large flares.

4. Energy Input to the Solar Atmosphere

Here we compute energy input rate from energetic particle collisional losses as a function of column density, under the simplifying assumption that the energetic particles are precipitated from high in the corona, vertically downward into the solar atmosphere in a column of constant cross-sectional area. More complex particle injection models, i.e., models with non-vertical magnetic configurations, with various injection heights or with various initial pitch angle distributions, could be incorporated into the computation, but the vertical case illustrates the general features well.

For the fast electrons we follow the method of Brown (1973), which takes into account the scattering of the electrons in pitch angle. The rate of energy input per unit volume is given by

$$I_B(N, t) = 1.0\times 10^7 n(N, t)[x(N, t)+0.55]\times \\ \times \frac{A}{a} C(\gamma)(1.1\times 10^{-17} N)^{-(\gamma+1)/2} \text{ ergs cm}^{-3} \text{ sec}^{-1}, \quad (8)$$

where $n(N, t)$ is the hydrogen number density at column density N and time t; $x(N, t)$ is the fractional ionization; a is the cross-sectional area in cm^2; $\mathrm{d}J/\mathrm{d}(h\nu) = A(h\nu)^{-\gamma}$ is the photon spectrum at time t, photons (cm^2 sec keV)$^{-1}$; $C(\gamma) = \gamma^2(\gamma-1)^2 B(\gamma-\frac{1}{2}, \frac{3}{2}) B(\frac{1}{3}, (\gamma+1)/2)$ is plotted in Figure 2. This expression differs from that of Brown (1973b) due to an error in his evaluation of the integral in his Equation (7). We have also evaluated the constants in terms of the X-ray spectrum.

In Figure 4 we have plotted the energy input per ambient particle. $\mathrm{d}\varepsilon/\mathrm{d}t = I_B/n$ as a function of $N(\text{cm}^{-2})$ for the 4 August 1972 event, using the reported Hα area nearest the time of the X-ray burst maximum. We have used a two power-law fit to the X-ray spectrum with a break at about 65 keV and an ionization fraction as estimated for flares (Brown, 1973a).

A similar computation can be performed for the energetic protons. Neglecting scattering in pitch angle and using the energy loss curves given by McGuire (1976) for hydrogen, we derive an energy loss function for the energetic protons in the 4 August 1973 event (also shown in Figure 4). We note here that even under the

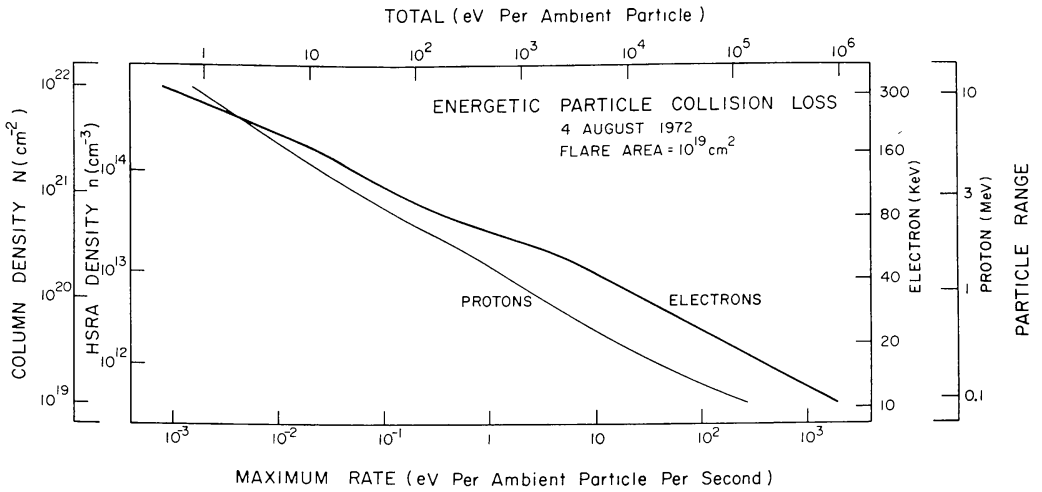

Fig. 4. The energy deposited in the solar atmosphere by energetic electrons and protons in the 4 August 1972 large proton flare is plotted here as a function of column density for a flare area of 10^{19} cm^2 and for the thick target model described in the text. The rate of energy deposition per ambient particle is given by the lower scale and the total energy deposited (flare duration ~ 500 sec) by the upper scale. The particle ranges are shown on the right. Note that the energy deposition for protons is substantially less than for electrons to a column density of $< 10^{21}$ cm^{-2}.

thick target approximation the energy lost by the protons is about 10 times less than the energy lost by the electrons for column densities of $\lesssim 3\times 10^{20}$ cm^{-2}, and 2 times less for column densities of $\lesssim 2\times 10^{21}$ cm^{-2}. Thus, the collisional energy losses of energetic protons are unlikely to be a major contributor to flare phenomena at those levels in the atmosphere, even under the most favorable thick-target models.

The total energy dumped at a given height z in the solar atmosphere is independent of the cross-sectional area a,

$$d\varepsilon = I_B(z)\Delta t a(z)\, dz,$$

$$d\varepsilon \approx -1\times 10^7 AC(\gamma)\Delta t[X(N)+0.55](1.1\times 10^{-17}\, N)^{-(\gamma+1)/2}\, dN. \qquad (9)$$

The total energy dumped below a given N was obtained by integration of Equation (9) and is shown in Figure 5 for each flare event. Except for the 4 August flare, a single power law has been fitted to the X-ray observations.

4.1. The radiative quasi-equilibrium region

Because the emissivity as a function of temperature has a peak and because the energy dumped into the solar atmosphere by the energetic particles increases with height, below some critical level the plasma will be able to maintain a quasi-equilibrium by radiating away the input energy. We define this critical level N_c by equating the rate of energy input which is a function of the column density N, with the rate of energy input necessary to maintain this maximum emissivity. For constant pressure the temperature for maximum emissivity is $T_c \approx 6\times 10^4$ K, with

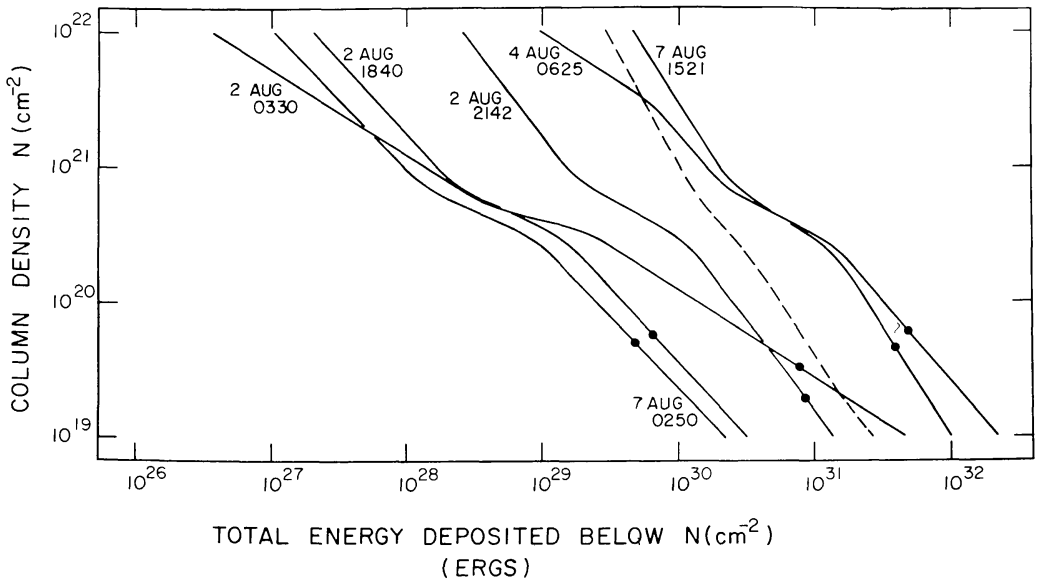

Fig. 5. The total energy deposited *below* a given column density by energetic electrons is plotted here for six flares of the August 1972 series. Also plotted is the proton energy deposition of the 4 August flare (dashed line). The dots indicate the dividing line between the radiative quasi-equilibrium region and the flare explosion region, i.e., the energy deposited below the dot goes primarily into radiation, and above to heating and mass ejection.

the radiation loss rate given by (Brown, 1973b)

$$\frac{dE_{rad}}{dt} \approx 1.9 \times 10^{-30}\, nN_c \text{ ergs cm}^{-3} \text{ sec}^{-1}. \tag{10}$$

This simple treatment assumes that the ionization level follows the temperature as in a hot, optically thin gas. Equating dE_{rad}/dt to I_B we find that

$$N_c = 9.1 \times 10^{16} \left[9.1 \times 10^{19} \frac{A}{a} C(\gamma) \right]^{2/(\gamma+3)} \text{ cm}^{-2}. \tag{11}$$

The values of N_c are indicated in Figure 5 for the maximum rate of electron energy input (at the hard X-ray maximum) using the reported Hα flare area nearest the time of X-ray maximum. ε_R, the total energy dumped into the radiative quasi-equilibrium region, is given in Table III.

4.2. The flare explosion

Above N_c the energy input rate will be too rapid for radiative equilibrium, and the ambient gas will rapidly increase in temperature and expand upward. At even higher levels of the atmosphere the energy gained by the ambient plasma may exceed that needed to escape the restraining forces of the Sun's gravitational and magnetic fields. This material will then be ejected from the Sun. If the velocity of the ejected material is sufficiently high, a shock wave will form in front. This shock wave can give rise to type II radio emission, and may be observed later as an interplanetary shock wave.

TABLE III

Comparison of observed flare energy output with energetic electron energy input[c] August 2–7, large proton flares

Flare phenomenon	0330 Aug 2 observed/computed	2058 Aug 2[a] observed/computed	0625 Aug 4 observed/computed	1522 Aug 7 observed/computed
I. Energetic particles				
a. >20 keV electrons at Sun	1×10^{31}	8×10^{30}	1.1×10^{32}	6×10^{31}
escaping to IP medium	$>2\times10^{26}$	$>1.5\times10^{27}$	1×10^{29}	6×10^{27}
b. >10 MeV protons at Sun	—	—	1×10^{29}	$>1\times10^{28}$
escaping to IP medium	2×10^{29}	1×10^{30}	8×10^{30}	3×10^{29}
II. Radiative quasi-equilibrium region				
a. white light continuum, $N\geqslant10^{20}$ cm^{-2}			—	$5\times10^{29}/6\times10^{29}$
b. H_α			1×10^{30}	1×10^{30}
c. Total all optical lines (estimate from H_α)			2.5×10^{31}	2.5×10^{31}
d. UV (estimate)			$\sim10^{31}$	$\sim10^{31}$
e. EUV			10^{31}	10^{31}
Total optical, UV, EUV radiation	$-/8\times10^{30}$		$5\times10^{31}/5\times10^{31}$	$5\times10^{31}/5\times10^{31}$
III. Flare explosion region				
a. Soft X-ray flare plasma — energy	6×10^{30}	6×10^{30}	3.6×10^{31}	1.5×10^{31}
a. Soft X-ray flare plasma — mass	1.2×10^{15}	1.4×10^{15}	8.5×10^{15}	3×10^{15}
b. Interplanetary shock wave — energy	8.8×10^{31}	4.6×10^{32}	1.1×10^{31}	3.8×10^{32}
b. Interplanetary shock wave — mass	3.4×10^{16}	1.1×10^{17}	1.6×10^{16}	9.4×10^{16}
Total energy	$1\times10^{32}/9.5$ keV[b]	4.7×10^{32}[a]	$1.5\times10^{32}/16$ keV[b]	$4\times10^{32}/5$ keV[b]
Total mass	$3.5\times10^{16}/>1.5\times19^{15}$	1.1×10^{17}	$2.5\times10^{16}/>1.5\times10^{15}$	$1\times10^{17}/>2\times10^{15}$

[a] This is a double hard X-ray event with no quantitative data available for the 1st event.

[b] The computed value is the low energy cutoff to the electron spectrum required to provide all the energy for the flare explosion.

[c] All units ergs of gms unless otherwise labelled.

We are able to set lower limits to the energy and mass involved in this flare explosion process. The total energy available above N_c depends on the shape of the particle spectrum at low energies. Present hard X-ray observations are almost completely limited to $\geqslant 20$ keV. On the other hand, the few available < 20 keV observations indicate that the electron spectrum extends to $\leqslant 5$ keV (Kahler and Kreplin, 1971; Peterson *et al.*, 1973; Lin, 1973), so that $\varepsilon_{\text{coll}}(> 20\,\text{keV}) - \varepsilon_R$ would be a very conservative lower limit to the flare explosion energy.

The total mass of material above N_c is just $M_c = N_c a/\eta$. This material presumably goes into the flare soft X-ray plasma and the mass ejected from the Sun. We argue later that M_c is a lower limit to the mass of that material.

5. Comparison With Observations

A comparison of the computed energy input (Figures 4 and 5) with the observed flare emissions will show whether energetic particles suffice as an energy source for these emissions and whether the propagation of these particles through the solar atmosphere suffices as an energy transport mechanism. In the radiative equilibrium region the temperature and ionization can be derived as a function of height in the chromosphere by equating the input energy with the radiative losses (Brown, 1973b; Canfield, 1974). However, in the interest of simplicity we have chosen to compare only with the total energy output from the radiative equilibrium region, and with white-light continuum emission. In the flare explosion region, we compare the energy and mass input to the energy and mass contained in the flare X-ray plasma and flare ejecta and shock wave (see Table III).

5.1. White light emission

Enhancements of approximately 5–50% of the continuum emission are occasionally observed near the flash phases of large proton flares (Svestka, 1966; McIntosh and Donnelly, 1972). No white-light observations were available for the 4 August flare, but the 1500 UT August 7 flare provided the best available observations of white light flare emission, both spectroscopic and photometric (Rust and Hegwer, 1975; Machado and Rust, 1974).

The temporal variation of the continuum emission of 7 August corresponded within seconds to those of the hard (60–100 keV) X-ray flux during the flash phase. Until approximately 1524 UT the white-light emission appeared in several small, bluish flare knots of dimension $\leqslant 3'' \times 5''$ and total area $\sim 4 \times 10^{17}$ cm^2. After the flash phase, from 1525 to 1537 UT, a moving flare wave, yellowish in appearance, was observed in white light. A total of approximately 10^{30} ergs was emitted in the continuum from 3900 Å to 6900 Å, 6×10^{29} ergs before 1525 UT. Rust and Hegwer (1975) note that the total continuum energy amounts to about $\frac{1}{3}$ the total flare Hα energy deduced by Zirin and Tanaka (1973).

Synchrotron emission by highly relativistic electrons has been proposed as the source of the white light continuum emission (Gordon, 1954; Severny, 1958; Stein

and Ney, 1963). We can approximate the total synchrotron emission in the 3900–6900 Å white light band from the formulas of Ginzburg and Syrovatskii (1964):

$$\frac{d\varepsilon}{dt} \approx 5.4 \times 10^{-12} (10^4 H)^{(\delta+1)/2} K \text{ ergs/sec}, \tag{12}$$

where H is the magnetic field strength in Oersteds (equivalently Gauss) and K, δ are defined by the power law electron spectrum $dN/dE = KE^{-\delta}$ erg^{-1}, where E is in ergs. This approximation is valid for $1.5 \leqslant \delta \leqslant 5$. Electron energies of >100 MeV are required for emission in the visible range for magnetic field strengths of $\leqslant 10^3$ Gauss (Švestka, 1970). There are no measurements of electrons of these energies for the 7 August flare, and it would certainly be inappropriate to extrapolate the measurements below 100 keV to above 100 MeV. However, Ramaty *et al.* (1976) find that the 1–10 MeV γ-ray continuum observed for the 4 August 1972 flare could be produced by an electron population at the Sun with a power law spectrum

$$\frac{dN}{dE} \approx \frac{2.1 \times 10^{37}}{n_i} E^{-2} \text{ erg}^{-1} \quad \text{for} \quad E > 1 \text{ MeV}, \tag{13}$$

where n_i is the ambient density in the γ-ray source region. For mutually consistent values of n_i and H in the solar atmosphere, e.g., $H = 10^3$ G for $n \geqslant 10^{14}$ cm^{-3}, $H \approx 10$ G for $n = 10^9$ cm^{-3}, the rate of synchrotron emission falls below the observed white light emission rate of $\sim 5 \times 10^{27}$ ergs/sec by several orders of magnitude. Ramaty *et al.* (1976) note that a better fit for the γ-ray continuum is obtained with an exponential spectrum. This would further reduce the amount of synchrotron emission in the visible range.

Najita and Orrall (1970) and Švestka (1970) suggested that white light continuum emission comes from the heating of the photosphere by energetic protons on electrons. Extrapolating the energy deposition curves (Figure 5) to the photosphere we find that electrons in the 7 August proton flare deposited a total of $\sim 3 \times 10^{28}$ ergs below an optical depth $\tau = 0.10$ ($N \sim 8 \times 10^{23}$ cm^{-2}) and $\sim 1.5 \times 10^{28}$ ergs below $\tau = 1.0$ ($N \sim 2 \times 10^{24}$ cm^{-2}) using the HSRA model (Gingerich *et al.*, 1971). There are no γ-ray observations during the flash phase of this flare, but in the 4 August proton flare the proton energy deposition was comparable in magnitude to that of the electrons in the August 7 flare, in these deep layers. The energy estimates for both the electrons and protons are likely to be too large since: (1) we have not taken into account steepening in the electron spectrum at energies greater than about 10^2 keV (as is observed in the 4 August 1972 event); and (2) we have used the August 4, 1972 γ-ray event for an estimate of the protons even though the 7 August event emitted about an order of magnitude fewer protons into the interplanetary medium. As pointed out earlier, most of the γ-ray emission was likely to have been produced much higher in the solar

atmosphere by protons in the process of escaping from the Sun. Thus, photospheric heating by energetic protons or electrons falls short by a factor of at least 20 to 40 of the energy required for the observed white light emission.

Machado and Rust (1974) noted that the spectrum of the continuum enhancement during the moving flare wave after 1525 UT was inconsistent with simple photospheric heating. Their detailed analysis of the line and continuum emissions indicated that they were produced by free-bound transitions of hydrogen at a temperature of ~ 8500 K and column density $\sim 10^{21}$ cm^{-2}. We suggest that the bluish emission from the flare knots (before 1525) comes from free-bound emission of chromospheric gas which has been non-thermally ionized by the energetic electrons (Hudson, 1972; 1973). Non-thermal ionization, which refers to the direct production of ion pairs by the energetic particles at the rate of one ion pair per $\varepsilon_0 \approx 32$ eV of energy loss, can be compared to collisional and radiative ionization. At the relevant temperature and ionization levels, only hydrogen is important, so we obtain for equilibrium

$$\frac{dn_e}{dt} = -\alpha n^2 x^2 + (\beta + I_B/\varepsilon_0 n)(1-x)n = 0 \tag{14}$$

where α is the recominbation coefficient, β represents the net radiative and collisional ionization, and I_B/ε_0 the non-thermal ionization. Thomas and Athay's (1961) approximation for ionization equilibrium in the chromosphere appears adequate for flares in the absence of non-thermal ionization (Canfield, 1974), and for the constant-pressure case given by Brown (1973b) we have

$$\left(\frac{x+x_m}{1-x}\right)\left(\frac{1.1+x^*}{1.1+x}\right) = \frac{T}{n^*T^*}\frac{(2\pi mk/h^2)^{3/2}\exp(-\varphi_i/kT)}{\frac{2T}{T_R}\exp\left[\frac{\varphi_i}{4kT}\left(\frac{T}{T_R}-1\right)\right]}, \tag{15}$$

where $*$ refers to the initial values; m, k, and h have their usual meanings, $x_m = 10^{-4}$ from metals, φ is the hydrogen ionization potential, and $T_R \equiv 6\times 10^3$ K. Using (14) and (15) we solve for β with $I_B = 0$, using α as given by McDaniel (1964). These α values for the recombination coefficient include three-body processes, which become important for low temperatures and high densities. Figure 6 compares β and $I_B/\varepsilon_0 n$ for various atmospheric levels and temperatures. Non-thermal ionization dominates for $T \lesssim 10^4$ K and $N \gtrsim 10^{20}$ cm^{-2} for typical flares.

We believe the white-light continuum is generated in the following way: energetic electrons heat and ionize the chromospheric material, with one ion pair created for each 32 eV of initial kinetic energy. The recombination of the electrons, if to the ground state, results in immediate re-ionization because of the large optical depth in the Lyman continuum. Only Balmer or Paschen continuum transitions result in a photon which escapes. Thus roughly one Balmer or Paschen photon is emitted per incident 32 eV of electron energy. The plasma must become highly overionized, beyond the degree normally appropriate to the temperature,

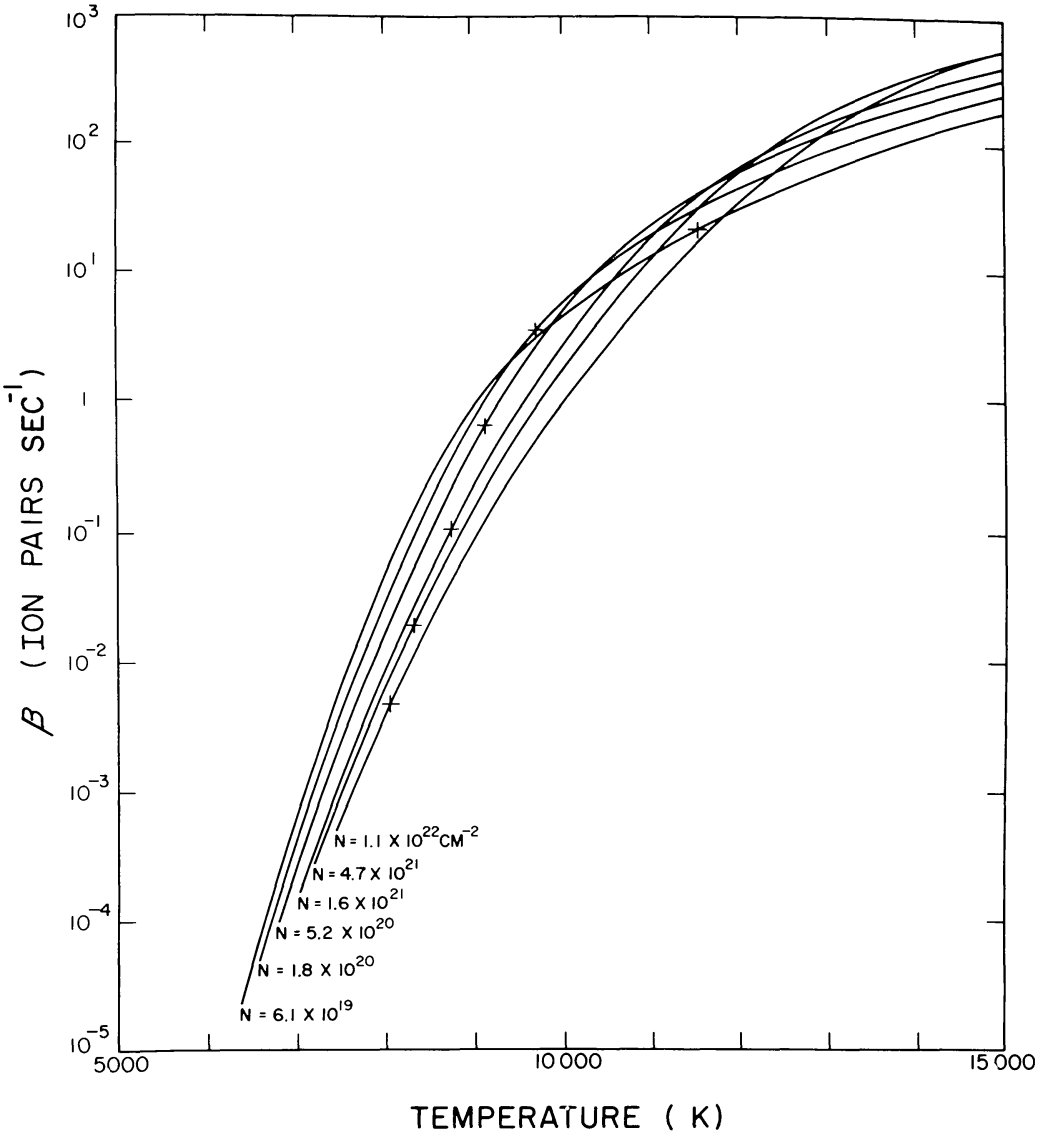

Fig. 6. β, the net collisional and radiative ionization coefficient (Equation 12) is shown here as a function of temperature for various HSRA levels under the Thomas and Athay (1961) chromospheric approximation to the ionization level. The crosses indicate the non-thermal ionization coefficient, I_B/ε_0, for the 1525 UT 7 August 1972 flare at the same levels. Thus non-thermal ionization dominates at temperatures below the crosses. For the temperature dependence with depth of a typical large X-ray flare (Brown, 1973b) non-thermal ionization dominates at $N \geqslant 10^{20}$ cm^{-2} and $T \leqslant 10^4$ K.

in order to increase its continuum emissivity until it balances the non-thermal ionization. The energy not appearing in Balmer and higher continua must, of course, appear in various bound – bound transitions, but these transitions do not change the ionization level.

The Paschen continuum must supply most of the 3900–6900 Å flux observed in the bluish knots. Since Paschen transitions are about $\frac{1}{3}$ as likely as Balmer transitions, the net energy conversion efficiency is $\sim\frac{1}{4}(3\text{ eV}/30\text{ eV})$ or $\sim 3\%$. Figure 5 shows that sufficient energy (2×10^{31} ergs) is deposited in the levels where non-thermal ionization dominates ($N \leqslant 10^{20}$ cm^{-2}) to account for the white light continuum emission.

The spectral distribution of the Paschen continuum depends upon the effective electron temperature. This cannot easily be computed because of the complexity of the radiation transfer and mass motion problems. It is quite reasonable, however, to expect temperatures on the order of 10^4 K. The difference in spectral distributions noted in the two phases of the white-light emissions in the August 7 flare – blue in the bright flare knots and red ($T \sim 8500$ K) in the moving wave – can be explained by different effective electron temperatures which result from the factor of ~ 10 difference in the intensity of precipitation.

The threshold for detection of white-light continuum enhancements is a $\sim 5\%$ increase above the quiet Sun. Since the 7 August flare had an increase of $\sim 50\%$ at 4950 Å we expect that flares with hard X-ray emission roughly an order of magnitude lower could still be detected in white light. This level corresponds to a total >20 keV electron energy of $\sim 5 \times 10^{30}$ ergs (Table III).

5.2. Total optical emission

The energy input to the radiative quasi-equilibrium region goes primarily into radiation in the visible, UV and EUV wavelengths. Zirin and Tanaka (1973) estimated the total emission in Hα to be $\sim 2 \times 10^{30}$ and 2.5×10^{30} ergs for the 4 and 7 August major flares, respectively, with about one-half of the total emission occurring during the flash phase. Ellison (1963) estimated that emission in other lines of the Balmer series at about 15 times the emission in Hα, and in all other emissions lines at about $10 \times$ Hα yielding a total of approximately 3×10^{31} ergs in visible line emission during the flash phase for the August 4 and 7 large flares.

Donnelly *et al.* (1973) and Donnelly and Hall (1973) found that the flash phase emission in the EUV region was dominated by chromospheric and transition region lines, implying that these emissions originate in the radiative quasi-equilibrium region. For the 7 August 1973 flare, Donnelly (private communication) estimates a total of $\sim 10^{31}$ ergs emitted in the 10-10^3 Å wavelength range during the flare impulsive phase. No measurements are available in the UV wavelength range 1000–3000 Å but we expect that its energy flux is of the same order of magnitude as that of the EUV. The total of about 5×10^{31} ergs in optical, UV and EUV emissions agrees within the estimation errors with the computed values (Table III) of energy dumped in the quasi-radiative equilibrium region for the 4 and 7 August large flares.

Among the smaller flares the 1840 UT August 2 flare was the most brilliant that Zirin and Tanaka (1973) report having ever observed in Hα. Correspondingly we find that at depths of $N \geqslant 10^{21}$ cm^{-2}, this flare had one of the highest rates of electron energy deposition per unit area (I_B) of any of the August flares because of its small area and short duration. Zirin and Tanaka also observed 3835 Å flashes coinciding with the X-ray bursts. The 3835 Å emitting layer was located at $N \geqslant 10^{20.3}$ and its maximum total radiative emission rate was estimated to be 2.6×10^{27} ergs/sec. We find that the energetic electron collision loss below a column density of $N \sim 4 \times 10^{20}$ cm^{-2} could have provided this energy.

The smallest optical flare of the 2 to 7 August period for which X-ray data were available was the sub-flare of approximately 0250 UT 7 August. It correspondingly had the smallest electron energy deposition (Figure 5).

5.3. The soft X-ray plasma

In the flare explosion region the fast-particle energy input goes primarily into heating and expansion of the atmospheric gas. A substantial portion of the heating needed to form the soft X-ray flare plasma may be due to this energy input. We note here the critical level of the solar atmosphere defined by N_c is located in the pre-flare chromosphere, implying that chromospheric material forms the X-ray flare plasma as a result of the explosive heating by the fast electrons. It should be noted, however, that significant growth of soft X-ray sources can occur in the absence of non-thermal X-rays (Datlowe, 1975).

For the August flares the emission measure, $n_e n_i V$, and temperature T, are available from soft X-ray measurements (Dere *et al.*, 1973; Neupert *et al.*, 1974). The total energy in the flare plasma can be obtained if the plasma density is known since

$$\varepsilon_{\text{plasma}} \approx e n_i V k T = \frac{3(n_e n_i) k T}{n_e}. \tag{16}$$

Assuming a typical density of $\sim 3\times 10^{10}\,\text{cm}^{-3}$ for the X-ray flare plasma we obtain a total energy ranging from 6×10^{30} to 4×10^{31} ergs (Table III). These energy requirements can easily be met by the energetic electron collisional energy loss in the flare explosion region. Radiation losses during the impulsive phase are negligible compared to the total plasma energy content.

5.4. The interplanetary shock wave

The amount of energy involved in the interplanetary shock wave can be estimated from the plasma density ρ, velocity v, temperature T and magnetic field B observed near 1AU,

$$\varepsilon_{\text{shock}} = \Omega R^2 \int [(\tfrac{1}{2}\rho v^3 - \rho_b v_b^3) + \varepsilon_g(\rho v - \rho_b v_b) + \tfrac{3}{2} k(\rho v T - \rho_b v_b T_b) + \frac{1}{8\pi}(B^2 v - B_b^2 v_b)]\, dt,$$

where the terms represent the flow, gravitational, thermal, and magnetic energy, respectively (the subscript b denotes the pre-shock background levels). $\varepsilon_g \approx 2$ keV is the energy per particle associated with the gravitational potential and ΩR^2 is the area subtended by the shock. Computations by Dryer *et al.* (1976), using Pioneer 9 plasma and assuming $\Omega = 2\pi$ steradians at 0.78 AU, show that the energy in these shock waves ranges from 1 to 5×10^{32} ergs (Table III). Note that shock waves only come from flares with >20 keV electron energy of 1×10^{31} erg or greater. The total shock wave energy can be supplied by the fast electrons if the

electron spectrum extends down to 10 keV, 14 keV and 5 keV for the 0330 UT 2 August, 4 August and 1500 UT 7 August flares, respectively. Hence the energy requirements of the shock wave could easily be satisfied by the non-thermal electrons; however, the decisive observations of <20 keV non-thermal X-rays are not available.

5.5. Mass balance

The material above the radiative quasi-equilibrium region goes to form the soft X-ray flare plasma and the interplanetary shock wave. The mass of the material above the level of N_c is given by $M_c \approx N_c a M_p$ where M_p is the proton mass (Table III). Our computed values for M_c range from a few times 10^{14} gms for the smaller flares up to about 2×10^{15} g for the large flares, compared with 10^{15} to 5×10^{16} g computed by Brown (1973b). These differences are due to several errors in the Brown calculation (Brown, private communication).

The calculated values of M_c are a factor of from 18–50 times smaller than the sum of the masses of material in the soft X-ray plasma $M_x = (n_e n_i V/n_e \eta)$ and in the interplanetary shock $M_s = \Omega R^2 \int \rho v \, dt$ (Table III). Several factors may be responsible for this difference:

(1) The electrons may be accelerated lower in the solar atmosphere. Since there is sufficient energy in the electrons, essentially all the material above the acceleration region will be ejected. The energy input to the radiative equilibrium region would not change noticeably, except very close to the acceleration region.

(2) The flux tubes are not vertical but flare out with height. For magnetic fields with their sources in the photosphere or below, the cross-sectional area of a loop would increase as a function of height. Since $M_c \propto a^{(\gamma+1)/(\gamma+3)}$, an increase of a factor of 10 in the area would yield a factor of ~ 5 increase in M_c.

(3) The configuration may be a loop structure in which case all the mass in the loop above N_c would be ejected. There is strong evidence from the ATM white-light coronograph pictures for loop configurations in the ejected material (Gosling *et al.*, 1974). Loop structures are also found in soft X-ray and EUV observations of flares (Neupert *et al.*, 1974).

(4) Brown (1973b) points out that the ejected material may drag considerable quantities of the surrounding atmosphere with it, as in atmospheric nuclear explosions (Colgate, 1965).

(5) Soft X-ray absorption (Somov, 1975) may heat the chromospheric gas and cause further evaporation.

In a more realistic model these effects may be sufficient to increase M_c to values comparable to the sum of the observed M_x and M_s. The soft X-ray plasma may be formed in the loops which are not ejected from the Sun, while the interplanetary shock may be driven by the loops where the hot plasma has sufficient energy to overcome the Sun's magnetic and gravitational fields. The initial magnetic configuration thus determines the fractions of mass trapped and escaping from the Sun.

6. Discussion

We have shown that for the large proton flares of August, 1972 the energy in electrons accelerated at the flash phase dominates the total flare energy. To see whether this finding is typical of large proton flares, we have examined the solar hard X-ray burst observations of the OGO-1 and -3 (Arnoldy *et al.*, 1968a, b; Kane and Winckler, 1969), AIMP-1 and -2, and IMP-4 ionization chamber experiments. These experiments can measure intense hard X-ray bursts without saturation, and over the period September 1964 to the end of 1968, 178 solar X-ray bursts were observed. The response to solar hard X-rays is described in detail in Arnoldy *et al.* (1968). In Figure 7 the maximum count rate of the solar hard X-rays (normalized to the OGO-3 ionization chamber) is plotted as a function of solar longitude. We have defined large proton events as those which emit >10 MeV protons with a maximum flux at 1 AU greater than 10 cm^{-2} sec^{-1}. Essentially every flare west of central meridian with an X-ray burst above about 250 NPS$\times 10^{-3}$ gave rise to a large proton event. This count rate corresponds to a total >20 keV electron energy deposition of 10^{31} ergs. Thus, the events above this threshold are comparable to the August, 1972 large proton flares. Although many intense X-ray events were observed from flares east of central meridian, only two (E04 and E25) were followed by large proton events. This east–west effect is well understood and is due to the limited angular extent of the propagation of the protons.

Reversing the correlation we find that of the twenty large proton events observed over the same period, ten were preceded by intense X-ray bursts; five were unassociated with either a flare on the visible solar disc or a hard X-ray burst, and thus presumably were from flares behind the west limb of the Sun; and five occurred when there were no hard X-ray observations. This one-to-one correlation indicates that large proton event flares are highly non-thermal in character, with the bulk of the flare energy going primarily into the acceleration of electrons to 10–10^2 keV energies.

We have shown that the energy contents of the electromagnetic emissions, gas heating, and mass ejection effects observed for the August, 1972 flares are quantitatively consistent with those available from a simple model of the collisional interactions of the energetic electrons within the solar atmosphere. The predicted energy losses as a function of depth in the solar atmosphere are also consistent with the nature of the observed phenomena, and the existence of white-light continuum emission provides evidence of non-thermal ionization by energetic particles.

In these large flares the explosive heating of the upper chromosphere and corona by fast electrons must provide much of the energy and mass to form the soft X-ray flare plasma and the interplanetary shock wave. From the six flare events examined (Figure 5) it appears that a total energy above N_c of $\sim 10^{31}$ ergs in >20 keV electrons is required for an interplanetary shock wave to be formed.

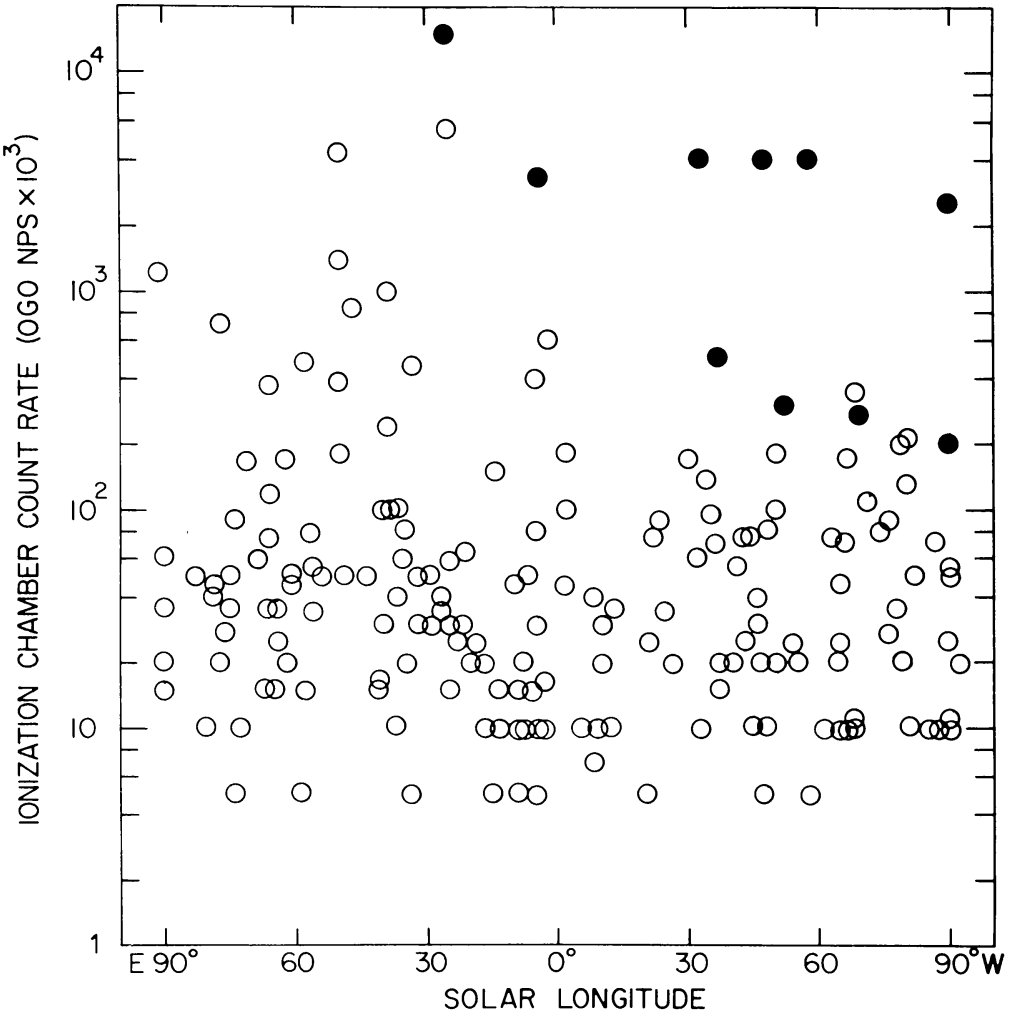

Fig. 7. The peak ionization chamber count rates for solar hard X-ray bursts observed from 1964 through 1968 are plotted here vs. the solar longitude of the associated flare. Flares which gave rise to proton events with >10 MeV fluxes above $10\,\mathrm{cm}^{-2}\,\mathrm{sec}^{-1}$ at 1 AU are indicated by the solid dots. Taking into account the E–W propagation effect, essentially all the flares with hard X-ray intensity above $250\,\mathrm{NPS}\times10^{-3}$ gave rise to such a proton event at 1 AU. Approximately 10^{31} ergs in >20 keV electron deposition is required for that count rate.

The energetic electron collisional losses appear sufficient by themselves to form a shock wave if the electron spectrum extends down to 5–10 keV.

Numerical simulation of shock propagation in the interplanetary medium (see Dryer, 1974 for review and Dryer *et al.*, 1975) shows that the time scale of the energy and mass perturbation to the quiet solar wind required to produce the observed shock effects is on the order of $\geqslant 10^{-2}$ the travel time to 1 AU (Hundhausen and Gentry, 1969). This time scale applies to the perturbation at the point where the solar wind flow becomes super-Alfvénic. The dynamic response of the solar atmosphere to the rapid ($\sim$minutes) input of electron energy to the upper chromosphere-lower coronal regions have yet to be analyzed in detail, but it seems physically reasonable that the resulting input at the super-Alfvénic boundary (probably located at 10–30 $R_\odot$) will occur over a time scale of about an hour.

Interplanetary shock waves are observed at 1 AU to be efficient accelerators of particles, particularly ions, to energies up to 1 to 10 MeV. These same shock waves traversing the stronger and more ordered magnetic fields near the Sun, could accelerate ions and electrons to relativistic energies in a second non-thermal phase in large flares. The γ-ray line observations, available essentially for only one flare (4 August 1972), indicate that the acceleration of protons and other nuclei is a sparate process from the flash-phase electron acceleration. Most of the protons escape to (or are accelerated in) the interplanetary medium, and produce the γ-ray emission while escaping, and the bulk of the proton acceleration appears to occur a few minutes later than the electron flash phase. Furthermore, the protons deposit substantially less energy in the solar atmosphere than the electrons, and thus are unlikely to be responsible for the observed emissions. The γ-ray observations and upper limits also show that Ellitott's (1964) flare hypothesis, for flare production by the sudden precipitation of high energy protons which were previously accelerated and stored in the solar corona, is not valid for these large proton flares.

Energetic solar flare protons are observed to be rapidly distributed over a wide range ($\sim 60°$) of solar longitude (Reinhard and Wibberenz, 1974; Van Hollenbeke *et al.*, 1975). This "fast propagation region" could be then identified with the region over which the shock wave accelerates particles. From radioheliograph measurements of solar type II radio bursts it is known that these shock waves typically propagate over a large extent in solar longitude.

Hence the differences between small flares and large proton flares may be explained by the ejection of material and the formation of a shock wave. By implication the energy input from electrons accelerated at the flash phase is insufficient in small flares to eject sufficient material to form a shock wave. The analysis of the August, 1972 flares and the correlation of Figure 7 indicate that a minimum of $\sim 10^{31}$ ergs energy in >20 keV electrons is required for producing a shock wave and large proton flare.

6.1. The flare mechanism

Even discounting the energy in <20 keV electrons, which we are not able to observe, the >20 keV electrons contain 10 to 50% of the total energy output for the August, 1972 flares. Thus, the flare mechanism for these large flares must be a very efficient accelerator of electrons. We are unaware of any applicable theoretical models for acceleration processes with such high efficiency. However, laboratory studies have shown that rapid and efficient energization of plasma electrons results through collective wave-particle interactions in plasmas carrying very large currents (Hamberger *et al.*, 1971). This situation occurs for current densities of $j = n_e e v_d$ corresponding to drift velocities greater than the electron thermal speed, $v_d \geqslant v_{th} \simeq (kT_e/m)^{1/2}$. Under these conditions the fluid (two-stream) instability occurs and the conductivity drops to the turbulent plasma value $\sigma =$

$0.5(m/M_p)^{1/3}\omega_{pe}$ (Buneman, 1959; Hamberger and Friedman, 1968), for a hydrogen plasma where ω_{pe} is the electron plasma frequency. The energy released in the rapid dissipation of the current in this region of anomalous resistivity goes into the bulk energization of the plasma electrons. With particle densities and magnetic fields comparable to those in solar flares, Hamberger *et al.* (1971) were able to achieve electron energization up to about 40 keV average energy, similar to the observed electron energies during the flare flash phase. They ascribe the electron energization to fluctuating plasma-wave fields which are built up by the current instability. Runaway beams or other strongly directional electron motions appear to be ruled out by the observations.

We suggest that these large proton flares, and many smaller energetic flares of the type studied in our previous paper (Lin and Hudson, 1975) result from the catastrophic dissipation of large currents in the solar atmosphere, brought about the sudden onset of anomalous resistivity triggered by an increase in current density. Large current densities may be found in current sheets between regimes of differing magnetic fields, viz. between oppositely directed fields in magnetic merging model or in field-aligned current (see Sweet, 1969, for review). As the current density increases, the threshold for current-driven ion-sound turbulence, $v_d \geqslant v_s = (kT_e/M_p)^{1/2}$, will be reached before the two-stream instability occurs. Ion-sound wave turbulence $\omega \leqslant \omega_{pi}$ (ω_{pi} = ion plasma frequency), will be generated which will lower the conductivity and thus increase dissipation of the current, but without providing efficient acceleration of electrons. Ion-sound turbulence heating may be the energy release mechanism for thermal portions of some flares, as for example the pre-heating observed in soft X-rays for many flares prior to the non-thermal phase. However, to achieve the *efficient* acceleration of electrons required by the observations discussed here, the increase in current density must be rapid enough to exceed the two-stream threshold before the current is dissipated by ion sound turbulence, or the ion sound turbulence must be damped by some other process.

The role of current-driven anomalous resistivity in magnetic field merging models for solar flares has been extensively discussed elsewhere (Sweet, 1969; Bratenahl and Baum, 1975). Here we emphasize that field-aligned currents also appear to be a plausable energy source for these flares. Large field-aligned currents can be built up in magnetic loops by the motions of the footpoints or they may pre-exist in the loops when they pop through the photosphere. These force-free currents result in a twisting of shear of the magnetic field. By examining the orientation of Hα features relative to the underlying photospheric field it is possible on some occasions to estimate the shear and thereby the stored energy (Nakagawa and Raadu, 1972). Tanaka and Nakagawa (1973) have studied the evolution of the magnetic field and its shear for the August flares and they find that there is sufficient stored energy in the force-free currents for those flares. In the August 7 flare they were able to derive the rate of energy released as a function of time in the flare from the rate of untwisting of the Hα features. At the

time of the flash phase the energy release rate was about 10^{30} ergs^{-1}, approximately the rate that is needed to accelerate electrons during the flash phase.

We arrive at the following tentative physical picture of flares. First energy is stored in coronal and chromospheric magnetic fields by the convective motions of the magnetic footpoints in the photosphere. This energy is stored in the form of field-aligned currents of current sheets along magnetic field boundaries. At the start of a flare the threshold for current-driven ion-sound anomalous resistivity is exceeded in some part of the current system, resulting in rapid energy dissipation. In energetic flares the current density must exceed the threshold for two-stream instability, so that efficient bulk energization of the plasma electrons to 10–10^2 keV energy occurs as the primary energy release mechanism. This produces the non-thermal flash phase. The accelerated electrons lose energy by collisions with the solar atmospheric gas, providing heating and ionization of the gas. Optical, UV and EUV radiation result where the electron collisional energy can be balanced by radiative losses. In the upper chromosphere and corona the energy input is too great to be balanced by radiation and an explosion occurs which forms soft X-ray plasma and possibly a shock wave. This shock wave accelerates protons, other nuclei and electrons to relativistic energies as it traverses the solar atmosphere.

Although energetic electrons dominate the energy released in the impulsive phases of large flares (this paper) and small flares (Lin and Hudson, 1971), there is substantial evidence that other forms of energy release must be operative in the flare precursor and main phase (Tanaka and Nakagawa, 1974; Datlowe, 1975).

We have chiefly discussed plausibility and energetic feasibility for our flare picture. It is clear that many critical observations need to be made; particularly X-ray measurements of the low energy, <20 keV, end of the accelerated electron spectrum; improved γ-ray measurements to define the energetic proton population; and spatially resolved hard X-ray measurements to pinpoint the location of the electron acceleration region. Detailed computation of the radiative losses including the effects of non-thermal ionization, and a quantitative analysis of the flare explosion and shock wave formation, using the derived energy input from energetic electrons, are also required. Finally observations of plasma-wave turbulence in flares would provide insight into the flare mechanism itself.

Acknowledgements

We wish to acknowledge extensive discussions with J. Brown, R. Canfield, R. Donnelly, M. Dryer, S. Kane, R. Ramaty and Z. Švestka. This research was supported in part by NASA Contract NAS 5-20838 and NASA Grant NGL 05-003-017 at UCB and NASA Contract NAS 5-11081 and NASA Grant NSG 7167 at UCSD

References

Arnoldy, R. L., Kane, S. R. and Winckler, J. R.: 1968a, *Astrophys. J.* **151,** 711.

Arnoldy, R. L., Kane, S. R. and Winckler, J. R.: 1968b, University of Minnesota, Cosmic Ray Technical Report CR-108.

Bratenahl, A. and Baum, P. J.: 1976, *Solar Phys.* **47,** 345.

Brown, J. C.: 1971, *Solar Phys.* **18,** 489.

Brown, J. C.: 1973a, *Solar Phys.* **29,** 421.

Brown, J. C.: 1973b, *Solar Phys.*, **31,** 143.

Brown, J. C. and Hoyng, P.: 1975, *Astrophys. J.* **200,** 734.

Buneman, O.: 1959, *Phys. Rev.* **115,** 503.

Canfield, R. C.: 1974, *Solar Phys.* **34,** 339.

Chupp, E. L., Forrest, D. J. and Suri, A. N.: 1973, in R. Ramaty and R. G. Stone (eds.), *High Energy Phenomena on the Sun*, NASA SP-342, p. 285.

Colgate, S. A.: 1965, *J. Geophys. Res.* **70,** 3161.

Datlow, D. W.: 1975, in S. R. Kane (ed.), 'Solar, Gamma-, X-, and EUV Radiation', *IAU Symp.* **68,** 191.

Dere, K. P., Horan, D. M. and Kreplin, R. W.: 1973, Collected Data Reports on August 1972 Solar Terrestrial Events, World Data Center A, UAG-78, part II, p. 298.

Donnelly, R. F. and Hall, L. A.: 1973, *Solar Phys.* **31,** 411.

Donnelly, R. F., Wood, Jr., A. T. and Noyes, R. W.: 1973, *Solar Phys.* **29,** 107.

Dryer, M.: 1974, *Space Sci. Rev.* **15,** 403.

Dryer, M., Smith, Z. K., Steinoltson, R. S., Mihalov, J. D., Wolfe, J. H. and Chao, J. K.: 1976, *J. Geophys. Res.*, **81,** 4651.

Elliott, H.: 1964, *Planetary Space Sci.* **12,** 657.

Ellison, M. A.: 1963, *Planetary Space Sci.* **11,** 597.

Frost, K. J.: 1974, paper presented at Solar Physics-Plasma Physics Workshop held at Stanford University, Sept. 17–20.

Frost, K. J. and Dennis, B. K.: 1971, *Astrophys. J.* **165,** 655.

Gingerich, O., Noyes, R. W., Kalkofen, W. and Cuny, Y.: 1971, *Solar Phys.* **18,** 347.

Ginzburg, V. L. and Syrovatskii, S. I.: 1964, *The Origin of Cosmic Rays.* Pergamon Press, p. 97.

Gordon, I. M.: 1954, *Doklady AN SSSR* **94,** 813.

Gosling, J. T., Hildner, E., MacQueen, R. M., Numro, R. H., Poland, A. I. and Ross, C. L.: 1974, *J. Geophys. Res.* **79,** 4581.

Hamberger, S. M. and Friedman, M.: 1968, *Phys. Rev. Lett.* **21,** 674.

Hamberger, S. M., Jancarik, J., Sharp, L. E., Aldcroft, D. A. and Wetherall, A.: 1971, *Proceedings International Conference Plasma Physics and Controlled Nuclear Fusion*, Vol. II, p. 37.

Hoyng, P.: 1975, Doctoral thesis, University of Utrecht, The Netherlands.

Hudson, H. S.: 1972, *Solar Phys.* **24,** 414.

Hudson, H. S.: 1973, in R. Ramaty and R. G. Stone (eds.), *High Energy Phenomena on the Sun*, NASA, SP-342, p. 207.

Hundhausen, A. J. and Gentry, R. A.: 1969, *J. Geophys. Res.* **74,** 2900.

Jackson, J. D.: 1962, *Classical Electrodynamics*, J. Wiley and Sons, N.Y.

Jefferies, J. T. and Orrall, F. Q.: 1961, *Astrophys. J.* **133,** 946.

Kahler, S. W. and Kreplin, R. W.: 1971, *Astrophys. J.* **168,** 531.

Kane, S. R.: 1974, in Gordon Newkirk, Jr. (ed.), 'Coronal Disturbances', *IAU Symp.* **57,** 105.

Kane, S. R. and Winckler, J. R.: 1969, University of Minnesota Cosmic Ray Technical Report, CR-135.

Lin, R. P.: 1973, in R. Ramaty and R. G. Stone (eds.), *High Energy Phenomena on the Sun*, NASA SP-342, p. 439.

Lin, R. P. and Hudson, H. S.: 1971, *Solar Phys.* **17,** 412.

Machado, M. and Rust, D. M.: 1974, *Solar Phys.* **38,** 499.

McDaniel, E. W.: 1964, *Collision Phenomena in Ionized Gases*, J. Wiley and Sons, p. 600.

McGuire, R. E.: 1976, Ph.D. Thesis, Physics Department, University of California, Berkeley.

McIntosh, P. S. and Donnelly, R. F.: 1972, *Solar Phys.* **23,** 444.

Najita, K. and Orrall, F. Q.: 1970, *Solar Phys.* **15,** 176.

Nakagawa, Y. and Raadu, M. A.: 1972, *Solar Phys.* **25,** 127.

Neupert, W. M., Thomas, R. J. and Chapman, R. D.: 1974, *Solar Phys.* **34,** 349.
Peterson, L. D., Datlowe, D. W. and McKenzie, D. L.: 1973, in R. Ramaty and R. G. Stone (eds.), *High Energy Phenomena on the Sun*, NASA, SP-342, p. 132.
Ramaty, R., Kozlovsky, B. and Lingenfelter, R. E.: 1975, *Space Sci. Rev.* **18,** 341.
Ramaty, R. and Lingenfelter, R. E.: 1975, in S. R. Kane (ed.), 'Solar Gamma, X-, and EUV Radiation', *IAU Symp.* **68,** 363.
Ramaty, R. and Wang, H. T.: 1975, *14th International Cosmic Ray Conference Proceedings*, **5,** 1635.
Reinhard, R. and Wibbernez, G.: 1974, *Solar Phys.* **36,** 473.
Roelof, E. C., Lezniak, J. A., Webber, W R., McDonald, F. B., Teegarden, B. J. and Trainor, J. H.: 1974, in D. E. Page (ed.), *Correlated Interplanetary and Magnetospheric Observations*, D. Reidel, Publ., p. 563.
Rust, D. M. and Hegwer, F.: 1975, *Solar Phys.* **40,** 141.
Severny, A. B.: 1957, *Izv. Krymsk. Astrofiz. Observ.* **17,** 129.
Somov, B. V.: 1975, *Solar Phys.* **42,** 235.
Stein, W. A. and Ney, E. P.: 1963, *J. Geophys. Res.* **68,** 65.
Švestka, Z.: 1966, *Space Sci. Rev.* **5,** 388.
Švestka, Z.: 1970, *Solar Phys.* **13,** 471.
Sweet, P. A.: 1969, *Annual Review Astron. Astrophys.* **8,** 149.
Tanaka, K. and Nakagawa: 1973, *Solar Phys.* **33,** 187.
Thomas, R. N. and Athay, R. G.: 1961, *Physics of the Solar Chromosphere*, Interscience Publishers.
Trubnikov, B. A.: 1965, *Rev. Plasma Phys.* **1,** 105.
Van Hollenbeke, M. A. I., MaSung, L. S. and McDonald, F. B.: 1975, *Solar Phys.* **41,** 189.
Wang, H. T. and Ramaty, R.: 1974, *Solar Phys.* **36,** 129.
Zirin, H. and Tanaka, K.: 1973, *Solar Phys.* **32,** 173.